Available online at www.sciencedirect.com
SCIENCE DIRECT®
International Journal of Multiphase Flow 30 (2004) 1037–1050
International Journal of Multiphase Flow
www.elsevier.com/locate/ijmulflow

Brief communication

A front tracking method for computations of boiling in complex geometries ☆

Asghar Esmaeeli *, Grétar Tryggvason

Department of Mechanical Engineering, Worcester Polytechnic Institute, Worcester, MA 01609, USA

Received 30 October 2003; received in revised form 14 April 2004

1. Introduction

While significant progress has been made in the last decade or so in direct simulations of multifluid systems without phase change, numerical techniques for direct simulations of flows with phase change have been developed more slowly. Computations of film boiling in two-dimensional systems include Son and Dhir (1998) using a level set method, Juric and Tryggvason (1998) using a front tracking technique, Welch and Wilson (2000) using a volume-of-fluid (VOF) method, and Esmaeeli and Tryggvason (2004a,b) using a front tracking technique. Simulations of three-dimensional systems are also emerging (Esmaeeli and Tryggvason, 2004a,b; Shin and Juric, 2002). In all of these simulations the hot surface is flat and the fluid is initially at rest.

Although boiling of quiescent fluids in simple geometries such as film boiling over a flat surface is often studied and sometimes encountered in practical situations, boiling more frequently takes place where the liquid is flowing and the geometry is complex. In this paper we take a first step to study such flows computationally by introducing a method that allows for incorporation of complex geometries into the flow field. To test the capabilities of the method we examine film boiling of an initially quiescent fluid on a horizontal cylinder and multiple cylinders and focus on heat transfer rates that are sufficiently high to sustain film boiling. Boiling from hot horizontal cylinders has many industrial applications, such as in heaters and heat exchangers. Although under normal operating conditions (i.e., modest wall superheat) the heat transfer is mostly due to nucleate boiling or natural convection, system failure may result in increased superheat and transition to film boiling. This is particularly true when the working fluid is a low boiling-point liquid such as oxygen.

☆ Dedicated to Prof. George Yadigaroglu on the occasion of his 65th birthday, recognizing his many contributions to multiphase flow research.

* Corresponding author. Tel.: +1-508-831-5462; fax: +1-508-831-5680.
E-mail address: aesmae@wpi.edu (A. Esmaeeli).

0301-9322/$ - see front matter
doi:10.1016/j.ijmultiphaseflow.2004.04.008

The progress made in simulating two-fluid flows, including the motion of many bubbles and drops, over the last decade has relied nearly exclusively on the use of the so-called "one-field" approach where a single set of governing equations is used to represent all the different fluids that are present. In this way, it is possible to use a single regular structured grid to resolve the motion. Although this introduces certain challenges in representing the fluid interface accurately, as grid lines generally do not coincide with the interface, experience has shown that the difficulties are far outweighed by the ease of which the rest of the computations can be carried out. All numerical simulations of boiling conducted so far have also used the one-field approach.

Currently, there is a growing interest in representing solid boundaries on regular structured grids as is evidenced by the number of publications in this area. The available techniques can be categorized into two main groups: (i) immersed boundary methods and (ii) cut-cell methods. In the former, a solid boundary is treated as a different phase and is represented on a regular structured grid in the same way as a phase boundary in one-field methods. This approach has a long history, but its modern incarnation goes back to Goldstein et al. (1993) who simulated single-phase flow around a solid cylinder by adding a regularized force, in an iterative way, to the momentum equation to keep the boundary in place. Several authors have since refined this approach, but the most important contribution is due to Fadlun et al. (2000) who showed that the velocity within a stationary rigid body represented as an immersed object on a regular grid can be set to zero without essentially any loss of accuracy. This approach was used by Al-Rawahi and Tryggvason (2002) for their simulations of dendrite solidification using a front tracking method. In the cut-cell methods, a Cartesian grid is used for all cells except those which are intersected by the boundary. The boundary cells are truncated so that they conform to the shape of the boundary surface and property jump conditions and interface boundary conditions at the boundary are treated as discontinuities. For a recent application of this method, see, for example, Kirkpatrick et al. (2003).

Here we introduce a front tracking/finite difference technique for simulating boiling flows in complex geometries. The method is similar to the one used by Esmaeeli and Tryggvason (2003, 2004a,b) to study explosive boiling in microgravity and film boiling on a horizontal flat surface and is a modification of the one used by Al-Rawahi and Tryggvason (2002) to account for the velocity boundary conditions on nonflat solid object. The new elements here are the implementation of a technique to specify the temperature of the embedded solid and the ability to handle three phases, solid, liquid and vapor (as well as an improved technique to allow three-dimensional breakup for tracked surfaces).

2. Formulation and numerical method

2.1. Mathematical formulation

Consider a domain consisting of a liquid and its vapor undergoing phase change. The material properties of the phases are different but constant within each phase. The governing equations describing the conservation of mass, momentum, and energy are written as one set of equations that are valid for the entire flow field. Away from the phase boundary, the one-field equations lead to the usual governing differential equations in each phase. At the interface, singular terms must

be introduced such that integrating these equations over an infinitesimal volume moving with the interface results in the proper jump conditions. Here, we assume that both the liquid and the vapor are incompressible and the only change of volume is due to phase change at the phase boundary. We also assume that the interface temperature T_f is the same as the saturation temperature at the system pressure, i.e., $T_f = T_{sat}(p_{sys})$. With these assumptions, the mass and the momentum conservation and the thermal energy balance equations in conservative form, valid for the entire flow field, are

$$\nabla \cdot \overline{u} = \frac{1}{h_{fg}}\left(\frac{1}{\rho_v} - \frac{1}{\rho_l}\right)\int_F \delta(\overline{x} - \overline{x}_f)\dot{q}_f \, dA_f, \tag{1}$$

$$\frac{\partial \rho \overline{u}}{\partial t} + \nabla \cdot \rho \overline{u}\overline{u} = -\nabla p + \rho \overline{g} + \nabla \cdot \mu(\nabla \overline{u} + \nabla \overline{u}^T) + \sigma \int_F \delta(\overline{x} - \overline{x}_f)\kappa_f \overline{n}_f \, dA_f, \tag{2}$$

$$\rho c T\left(\frac{\partial T}{\partial t} + \nabla \cdot \overline{u} T\right) = \nabla \cdot k \nabla T - \left[1 - (c_v - c_l)\frac{T_{sat}}{h_{fg}}\right]\int_F \delta(\overline{x} - \overline{x}_f)\dot{q}_f \, dA_f. \tag{3}$$

Here, δ is a two- or three-dimensional delta function which is constructed by repeated multiplication of one-dimensional delta functions. $\overline{x}$ is the point at which the equation is evaluated and $\overline{x}_f$ is the position of the front. Quantities with the subscript 'f' are evaluated at the front. $\overline{u}$ is the velocity, $\overline{n}$ is a unit vector normal to the phase boundary pointing toward the vapor, p is the pressure, ρ is the density, μ is the viscosity, $\overline{g}$ is the gravity, T is the temperature, c is the heat capacity, k is the heat conductivity, σ is the surface tension, h_{fg} is the latent heat of evaporation, and $\dot{q}$ is the heat generation at the phase boundary as a result of phase change. Notice that these equations contain implicitly the conventional jump conditions for mass, momentum, and energy across the interface. For a more extensive discussion of this approach, see, Esmaeeli and Tryggvason (2004a).

2.2. Numerical method

The numerical method for the current study is similar to the one used by Esmaeeli and Tryggvason (2004a) to simulate film boiling on flat surfaces. Eqs. (1)–(3) are solved by a second order space-time accurate front tracking/finite difference method on a staggered grid. The time integration proceeds in two steps using a predictor–corrector scheme. As the basic method has been described in detail by Esmaeeli and Tryggvason (2004a), we only outline it briefly and focus on the changes that have been made to include embedded solid boundaries. Here we discuss a first order time integration and refer the reader to Esmaeeli and Tryggvason (2004a) for detail of the modifications that make the scheme second order.

The vapor and the liquid region are identified by an indicator function I which is unity in the vapor and zero in the liquid. The vapor/liquid boundary changes with time and must be reconstructed at every time step. This is done by a technique described in Tryggvason et al. (2001) where the indicator function is reconstructed from the front position. The fluid properties $\phi^n \equiv (\rho^n, \mu^n, k^n, c^n)$ are then found by

$$\phi^n = \phi_v I^n + \phi_l(1 - I^n), \tag{4}$$

where superscript n refers to the current time. The normal velocity of the phase boundary, $u_n = \overline{u}_f \cdot \overline{n}$, can be found from mass and energy jump conditions (Esmaeeli and Tryggvason, 2003)

$$u_n = \frac{1}{2}(\overline{u}_l + \overline{u}_v) \cdot \overline{n} - \frac{\dot{q}_f}{2h_{fg}}\left(\frac{1}{\rho_l} + \frac{1}{\rho_v}\right), \tag{5}$$

where $\overline{u}_l$ and $\overline{u}_v$ are the velocities of the liquid and the vapor at the phase boundary. To move the phase boundary, we integrate $d\overline{x}_f/dt = u_n\overline{n}_f$ in time using a simple first-order integration method. The new position of the interface points are given by $\overline{x}_f^{n+1} = \overline{x}_f^n + \Delta t u_n \overline{n}_f$. The indicator function at the new position I^{n+1} is then computed from the new position of the front (i.e., $\overline{x}_f^{n+1}$) and the density and the heat capacity fields at the next time step, ρ^{n+1}, c^{n+1}, are found. The energy equation (3) in a semi-discretized form is

$$\rho^n c^n \left(\frac{\widehat{T}^{n+1} - T^n}{\Delta t}\right) = \mathscr{A}^n, \tag{6}$$

where $\mathscr{A}$ represents the right hand side of equation (3), containing the advection, the diffusion, and the source term for the latent heat. In this equation the temperature at the next time step is identified as $\widehat{T}^{n+1}$ rather than T^{n+1}, since T^{n+1} must be corrected inside and at the boundary of the embedded solid in order to enforce the boundary condition for the temperature at the surface. To account for the solid boundary, we define another indicator function S, zero inside the solid and one in the rest of the domain, and use it to modify the temperature field

$$T^{n+1} = T_w(1 - S) + \widehat{T}^{n+1}S. \tag{7}$$

Here, S and I change smoothly from one phase to the other over about three grid blocks. Beckermann et al. (1999) and Al-Rawahi and Tryggvason (2002) found that pushing the transition zone toward the solid by using S^2 (instead of S) lead to better results.

Similarly, to account for the solid region in the momentum equation and to enforce no-slip/no-through flow condition at the solid boundary, we use S to set the velocity there equal to zero. This results in a slight modification of the standard projection scheme. In semi-discretized form the momentum equation is

$$\frac{\rho^{n+1}\overline{u}^{n+1} - \rho^n\overline{u}^n}{\Delta t} = -\nabla p + \mathscr{B}, \tag{8}$$

where the advection, the diffusion, the gravitational body force, and the surface tension force are denoted by $\mathscr{B}$. We then use a projection method and split the above equation into

$$\frac{\rho^{n+1}\overline{u}^{**} - \rho^n\overline{u}^n}{\Delta t} = \mathscr{B} \tag{9}$$

and

$$\frac{\rho^{n+1}\overline{u}^{n+1} - \rho^{n+1}\overline{u}^{**}}{\Delta t} = -\nabla p. \tag{10}$$

Here, $\overline{u}^{**}$ is a provisional velocity field which is computed from equation (9) is corrected to set the velocity inside the solid to zero

$$\overline{u}^{*} = S\overline{u}^{**}. \tag{11}$$

In the second step, $\overline{u}^{**}$ in Eq. (10) is replaced by $\overline{u}^{*}$ and an equation is found for the pressure by taking the divergence of the resulting equation

$$\nabla \cdot \frac{1}{\rho^{n+1}} \nabla p = \frac{\nabla \cdot \overline{u}^{*} - \nabla \cdot \overline{u}^{n+1}}{\Delta t}. \tag{12}$$

Next, we replace $\nabla \cdot \overline{u}^{n+1}$ term in the above equation with the right-hand side of Eq. (1). The resulting pressure equation is then solved by a multigrid solver developed by Adams (1989). The velocity at the next time step is found from Eq. (10) by replacing ∇p by $S\nabla p$ and $\overline{u}^{**}$ by $\overline{u}^{*}$. While in Esmaeeli and Tryggvason (2004a,b) we used a central difference method to discretize the advection terms in the momentum and the energy equations, here, we have used a QUICK scheme (Leonard, 1979) in order to be able to simulate flows at high Grashof number.

Interface merging and break up is an inherent characteristics of boiling flows. While the physics of topology change is far from trivial and still a matter of ongoing studies, we allow topology change to take place when the centroid of two opposing elements are less than two grid blocks ($2h$) apart. In two dimensions, this is achieved by computing the distances between the centroids of the elements and performing a local surgery at the interface if a distance is less than $2h$. For three dimensional systems, we use a level contour method similar to Shin and Juric (2002) and reconstruct the phase boundary by using the contours of the indicator function. While Shin and Juric (2002) do this reconstruction at every 100 time steps or so, we do it only when we are certain that a topology change is going to take place. To achieve this, we look for close elements at every 100 time steps using a fast method. We divide the computational domain into several blocks using a very coarse grid (i.e., 10–15 grid points in each direction) and store the coordinates of the centroid of the front elements at the points of this grid. Next, we compute the distances between the centroids of elements that have the same grid index as well as the distance between their centroids and those of their immediate neighbors on the grid. If the distance is less than $2h$, a flag is raised to proceed with interface reconstruction. Also, contrary to Shin and Juric's (2002) approach, in our code the front elements are always logically connected. This calls for an algorithm to set the new connectivities between the elements after a topology change and is achieved by a method similar to the fast search operation.

3. Results

The numerical method and the code, in the absence of solid boundaries have been validated extensively by comparing our results with available numerical, analytical, and experimental results. These comparisons are documented in detail in Esmaeeli and Tryggvason (2004a,b, 2003). Here, we present two new tests to check the accuracy of the method with embedded solid boundaries. These tests examine the accuracy of the energy solver and the flow solver, respectively. We then present a simulation of film boiling over a horizontal cylinder for a three-dimensional system and a highly unsteady film boiling on multiple two-dimensional cylinders. These examples test the full phase change algorithm and illustrates the ease in which our method handles interface merging and break up.

3.1. Conduction heat transfer around a heated cylinder

In this test, we solve for the temperature field in an annular region between two infinitely long concentric cylinders. The radii of the cylinders are R_1 and $R_2 > R_1$ and initially both are at T_0. At time $t = 0$, the temperature of the inner cylinder is raised to $T_w > T_0$. The evolution of the temperature is governed by

$$\frac{1}{\alpha}\frac{\partial T}{\partial t} = \frac{\partial^2 T}{\partial r^2} + \frac{1}{r}\frac{\partial T}{\partial r} \tag{13}$$

subject to the following initial and boundary conditions; $T(r,0) = T_0$, $T(R_1,t) = T_w$, and $T(R_2,t) = T_0$. An analytical solution to this problem can be found in a number of classic heat transfer textbooks. See, for example, Ozisik (1980), for a transient solution, and Incropera and DeWitt (2002), for a steady-state solution. To simulate this problem, we chose a 1×1 domain, $R_1 = 0.15$, $R_2 = 0.4$, $\rho = 0.2$, $k = 0.1$, $c = 1$, $T_0 = 0$, and $T_w = 1$ and resolved the flow by a 32^2, 64^2, 128^2, and 256^2 grid. The cylinders were described by smoothed indicator functions and the initial temperature field was assigned using the indicator functions I and S. To compute the net heat flux we could proceed in two ways. We could find the temperature gradient at the wall of the solid cylinder and integrate over its circumference. Since the cylinder is represented on a fixed grid by smoothed indicator function, this required carefully approximating the temperature gradient near the surface. While this could be done, a simpler approach was to use energy balance on a control volume that includes the cylinder and then find the heat necessary to keep the cylinder hot

$$\dot{Q} = \frac{\partial}{\partial t}\int_{\forall} \rho c T \mathrm{d}v + \oint_A k\frac{\partial T}{\partial n}\mathrm{d}A. \tag{14}$$

We calculated the instantaneous heat loss using the original solid indicator function S and two of its variants S^2, and S^4 and the best results were obtained for S^4. The net heat loss versus time using the finest grid is shown in Fig. 1 along with the exact analytical results. The dashed line shows the

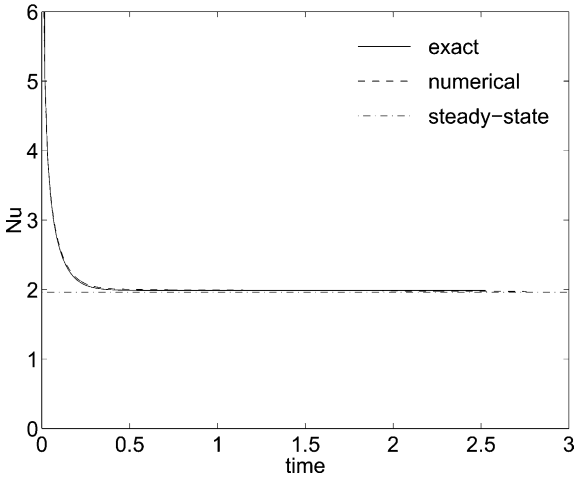

Fig. 1. Variation of nondimensional temperature gradient (at the surface of a heated cylinder) with time.

steady-state heat loss. The relative error at steady-state for the above grid resolutions are 6.50%, 3.71%, 1.364%, and 0.64%, respectively.

3.2. Pressure-driven flow over periodic array of long parallel cylinders

To test the flow solver, we repeated the test used by Al-Rawahi and Tryggvason (2002) where they simulated pressure-driven flow over square array of infinitely long parallel cylinders at different solid fractions c. For Stokes flow, Sangani and Acrivos (1982) and Drummond and Tahir (1984) found analytically the drag force per unit length of each cylinder, F. Their expressions, which differ slightly but give essentially the same numerical result at low solid fractions (where they are valid), are

$$F = 4\pi\mu U\left[-\frac{1}{2}\ln c - 0.738 + c - 0.887c^2 + 2.038c^3\right]^{-1}$$

and

$$F = 8\pi\mu U\left[\ln\left(\frac{1}{c}\right) - 1.47633597 + \frac{2c - 0.79589781c^2}{1 + 0.48919241c - 1.60486942c^2}\right]^{-1},$$

respectively. Here, U is the mean fluid velocity and the average pressure gradient is related to the drag force by $F/L^2 = \mathrm{d}p/\mathrm{d}x$, where L is the size of the domain. For our test, we took a 1×1 domain (i.e., $L = 1$) and cylinders of radii $0.1 - 0.35$ with incremental radius of 0.05. Other variables were $\rho = 1$, $\mu = 1$, and $\mathrm{d}p/\mathrm{d}x = 1$. For these parameters the Reynolds number $Re = \rho UD/\mu$ is $O(10^{-2})$ and the Stokes flow assumption can be expected to be valid. We carried out simulations at grid resolutions of 64^2, 128^2, and 256^2 and for solid indicator functions S, S^2, and S^4. Again, the best results were obtained for S^4. In Fig. 2 we compare the numerical mean velocity at the finest grid, nondimensionalized as $\widetilde{U} = U\mu/F$, with the analytical results. The

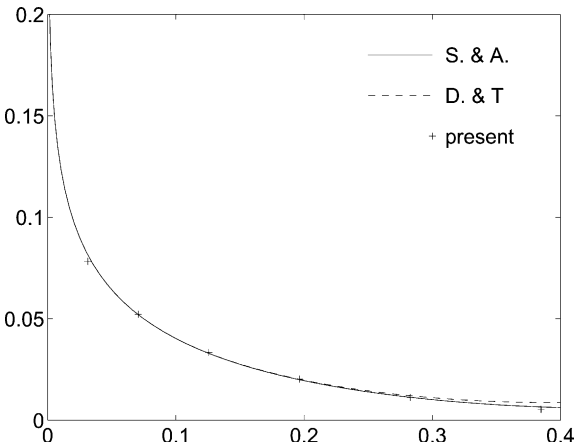

Fig. 2. Variation of nondimensional steady-state mean velocity with solid fraction. The numerical results were obtained by running the simulations till the steady-state. The analytical results correspond to Sangani and Acrivos (1982) and Drummond and Tahir (1984).

relative error at solid fraction of 0.03 for the above grid resolutions are 10.89%, 4.83%, and 2.24%, respectively. At this solid fraction, there are about 13, 26, and 39 points per cylinder diameter.

3.3. Film boiling on a horizontal cylinder

We now turn to the more challenging problem of film boiling on horizontal cylinders. Here, a hot cylinder, blanketed by a thin vapor layer, is immersed in a pool of liquid. Initially, both the liquid and the vapor are at a saturation temperature and the flow is quiescent. The gravitational acceleration is downward and as the liquid evaporates, buoyancy results in the formation of a vapor bubble on the top of the cylinder. At low wall superheats, bubbles are periodically released from the phase boundary, but at higher superheats, a steady vapor jet is formed.

Film boiling is characterized by the formation and release of bubbles at the phase boundary as a result of Rayleigh–Taylor instability. For film boiling on large flat plates, disturbances shorter than the critical Rayleigh–Taylor wavelength λ_c are stable and disturbances of length equal to the most unstable wavelength λ_{d2} grow most rapidly. For film boiling on circular cylinders, λ_{d2} also depends on the cylinder diameter. This dependency has been studied using analytical models (see, for example, Lienhard and Sun, 1970). The net result is that for constant operating conditions, the most unstable wavelength for a cylinder λ_{d2_c} is lower than λ_{d2} for small and moderate cylinders and asymptotes to λ_{d2} for very large cylinders.

Experimental and analytical studies on film boiling on horizontal cylinders are relatively plentiful. Bromley (1950) was probably the first to obtain a heat transfer coefficient for film boiling on a horizontal cylinder. His analysis, assuming that buoyancy is balanced by viscous forces, lead to the following expression for the Nusselt number:

$$Nu_B = 0.62(GrPr/Ja)^{1/4}, \tag{15}$$

where $Nu = -(D/\Delta T)\partial T/\partial y|_w$, $Ja = c_v\Delta T/h_f g$, $Gr = \rho_v g(\rho_l - \rho_v)D^3/\mu_v^2$ and $Pr = \mu_v c_v/k_v$. Bromley obtained the lead constant in the above equation from experimental data. Although Bromley did not consider $\widetilde{D} = D/l_s$ (D is the tube diameter and $l_s = \sqrt{\sigma/(\rho_l - \rho_v)g}$ is a capillary length) as an independent parameter, he stated that his correlation would not be valid for cylinders of very small or very large diameter. The effect of $\widetilde{D}$ was included by Breen and Westwater (1962) who conducted experiments with tubes of various sizes and proposed a new correlation

$$Nu_{BW} = (0.3727 + 0.2738(1/\widetilde{D}))(GrPr/Ja)^{1/4} \tag{16}$$

for a relatively large range of $\widetilde{D}$. For a more detailed discussion, see, Carey (1992).

3.3.1. Simulation of a three-dimensional system

We consider a two-phase fluid with the following thermophysical properties

$$\rho_l/\rho_v = 40, \quad \mu_l/\mu_v = 10, \quad k_l/k_v = 40, \quad c_l/c_v = 2, \quad h_{fg} = 10 \text{ kJ/kg}, \quad \sigma = 0.1 \text{ N/m},$$
$$T_{sat} = 500 \text{ K}.$$

These properties are the same as those used by Shin and Juric (2002) for their film boiling simulations on a horizontal flat plate. The calculations in Fig. 3 were performed in a computational domain of size $(W_x, W_y, W_z) = (0.06, 0.06, 0.15)$ resolved by a $64\times64\times160$ grid and a wall tem-

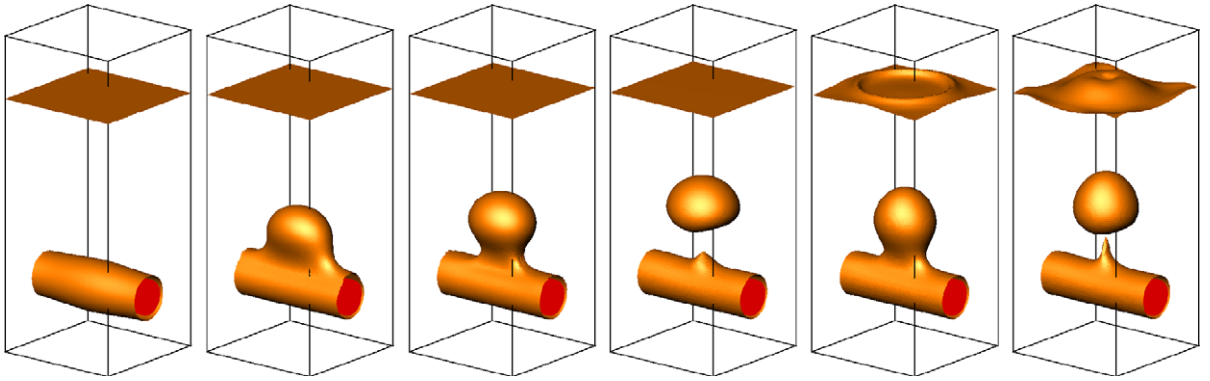

Fig. 3. A simulation of film boiling on a horizontal cylinder. Here $\rho_l/\rho_v = 40$, $\mu_l/\mu_v = 10$, $k_l/k_v = 40$, $c_l/c_v = 10$, $h_{fg} = 10$ kJ/kg, $T_{sat} = 500$ K and $T_w = 510$ K. The domain size is $0.06\times0.06\times0.15$ and is resolved by $64\times64\times160$ grid We include a second interface near the top of the domain through which the raising bubbles break.

perature of $T_w = 510$ K. The first frame shows the initial setup where a heated cylinder of diameter 0.016 is placed midway between the $x = 0$ and $x = 0.06$ planes. The initial phase boundary is a concentric cylinder of radius

$$r(y) = r_0 + \epsilon\cos(2\pi N y/W_y), \tag{17}$$

where $r_0 = 0.0112$, $\epsilon = -7.5\times10^{-4}$, and $N = 1$. This perturbation results in a symmetric wave with maximum amplitude in the middle of the cylinder. Periodic boundary conditions are imposed on the horizontal direction, no-through-flow boundary conditions are imposed on the lower boundary, and all the gradients set to zero at the upper boundary to allow for volume expansion as a result of evaporation. We also include another vapor layer on top of the liquid layer to allow rising bubbles (or steady jets) to break through. The remaining frames of the figure show the evolution of the phase boundary. Since buoyancy pulls the vapor film upward, the upper half portion of the film starts to thicken while the lower half portion of it becomes thinner. The hot cylinder wall, however, prevents the lower half from becoming too thin and film settles to an equilibrium thickness. As the top portion of the phase boundary grows larger, a bubble starts to from and eventually is pinched off. As soon as the bubble breaks up, surface tension pulls the interface back and the process repeats itself (frames 4–6). The coalescence of the bubble with the upper surface creates capillary waves (frames 5–6) which eventually die off.

3.3.2. A grid resolution test

To test the convergence of the method under grid refinement, we pick a two-dimensional system of size 0.08×0.16 and resolve it by 128×256, 256×512, and 512×1024 grids. Here, the parameters are the same as in Fig. 3 except $\rho_l/\rho_v = 100$ and $T_w = 520$ K. The top frames of Fig. 4 compares the interfaces at at an early and a late time. The agreement between the interfaces at the two finest grids are excellent and the overall agreement between the interfaces at other grids are good. The bottom frame shows the Nusselt number (i.e., nondimensional wall heat flux) for these runs. It is obvious that the heat fluxes at the two finest grids are very close.

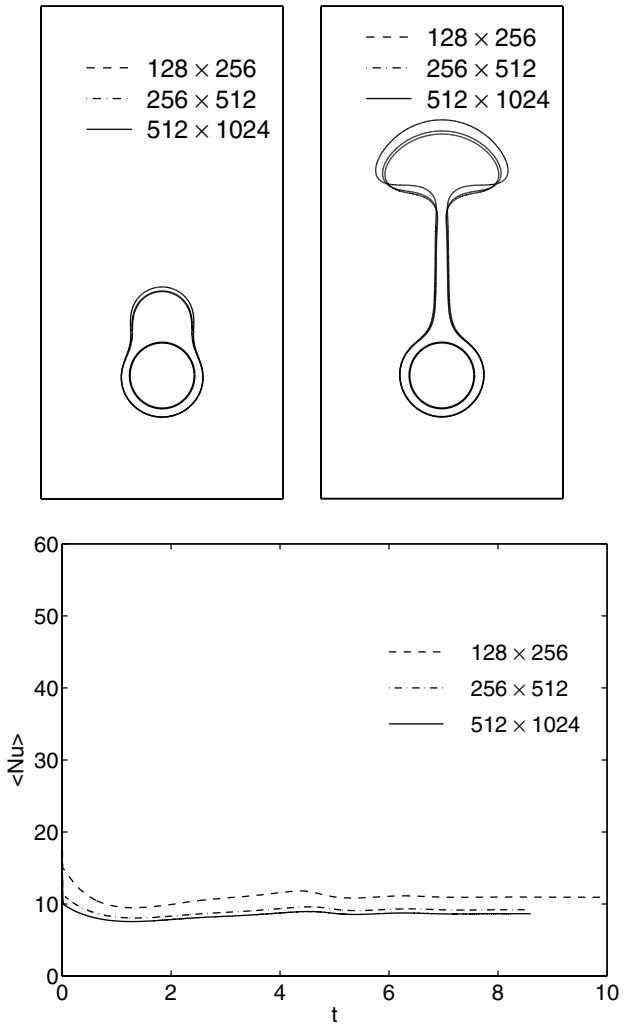

Fig. 4. A grid resolution test for film boiling on a horizontal cylinder. The top frames show the phase boundaries at $t = 2.14$ and 7.50, respectively, and the bottom frame shows the Nusselt number (i.e., nondimensional wall heat flux) versus time.

Here, steady-state $Nu = 8.63$ for the finest grid and Bromley's and Breen and Westwater's correlations predict $Nu_B = 7.45$ and $Nu_{BW} = 5.58$, respectively. The difference between the experimental correlation and the numerical prediction is—we believe—primarily due to differences between interface evolution in a two-dimensional system and a fully three-dimensional one (assuming, of course, that the correlations are reasonably accurate). In three dimensions, bubbles are released along the length of the tube with spacing that is mostly determined by surface tension. For a two-dimensional system, however, there is only one cylindrical bubble and the effect of surface tension is much smaller. In the limit of very small surface tension, we expect the vapor to leave as a thin jet from the top of the cylinder (although the possibility of multiple jets also exists)

and for high surface tension we expect the cylindrical liquid/vapor phase boundary to grow into an elliptical shape with the solid cylinder near its lower end. The shape of the jet in the low surface tension limit is likely to be determined by parameters other than surface tension and we would, therefore, expect that the vapor removal in two dimensions, unlike three dimensions, to be essentially independent of surface tension.

3.3.3. Effect of the wall superheat

The observed periodic bubble pinch off in Fig. 3 is determined to a large extent by the magnitude of the wall superheat. Experimental studies show that as the wall superheat increases, the frequency of bubble formation and the bubble size increase. Once the diameter of the vapor plume becomes sufficiently thick, the plume may not readily break up and eventually a vapor jet is formed. The wall heat flux increases with an increase in the wall superheat which translates to a reduction of the Nusselt number with an increase in the Jacob number. For both laminar and turbulent film boiling on horizontal cylinders, most of the correlations predict that $Nu \sim Ja^{-1/4}$ (Capone and Park, 1970).

To explore the variations of the wall heat flux with changes in the wall superheat, we have performed a few simulations for two-dimensional systems at several different wall superheats corresponding to $0.0427 \leqslant Ja \leqslant 2.14$. For this study, we consider a fluid with the following thermophysical properties

$$\rho_l/\rho_v = 4.78, \quad \mu_l/\mu_v = 2.59, \quad k_l/k_v = 3.55, \quad c_l/c_v = 0.55, \quad Pr = 4.2.$$

Other parameters are $Gr = 1680$, $Ja = 0.0426$, and $\widetilde{D} = 1.55$. Except for the Grashof number, the above thermophysical properties are close to those of saturated water at $p_{sat} = 169$ bar. The lower Grashof number implies a more viscous fluid or an acceleration higher than the normal gravitational acceleration (such as that in a rocket engine). However, it reduces the computational cost by reducing the grid resolution requirement (Esmaeeli and Tryggvason, 2004b). We used a 1.5×3 domain for $Ja \leqslant 0.0854$ and a 1.5×4 domain for $Ja > 0.085$ to accommodate the faster vapor generation. The grid resolution was 192×384 and 192×512, respectively. In Fig. 5 we plot $\overline{\langle Nu\rangle}$ versus Ja for these runs along with Breen and Westwater's correlation. Here, $\langle Nu(t)\rangle = 1/2\pi \int_0^{2\pi} Nu(\theta,t)\mathrm{d}\theta$ is the space-averaged Nusselt number, averaged over the surface area of the cylinder, and $\overline{\langle Nu\rangle} = 1/\Delta t \int_{t_i}^{t_e} \langle Nu(t)\rangle \mathrm{d}t$. t_i is the beginning of the quasi-steady-state and t_e is the endtime of the simulation. $\overline{\langle Nu\rangle}$ for the first two runs was calculated using the above expressions, but since $\langle Nu\rangle$ remained constant after the jet formation, $\overline{\langle Nu\rangle}$ is simply equal to $\langle Nu\rangle$ at the steady-state. At low Jacob numbers, the rate of decrease of $\overline{\langle Nu\rangle}$ is fast but it saturates as the Jacob number is increased. While the numerical results and the predictions by the correlation are different, they both show a similar trend.

3.4. A more complex example

To show the strength of our method in handling cases where the phase boundary is highly convoluted, we have simulated film boiling over multiple cylinders at a high wall heat flux. Here, the thermophysical properties are the same as in Section (3.3.3) except for $Gr = 67.2$ and $Ja = 1.06$. The computational domain is 2.8×5.6 and is resolved by a 128×256 grid. Fig. 6 shows

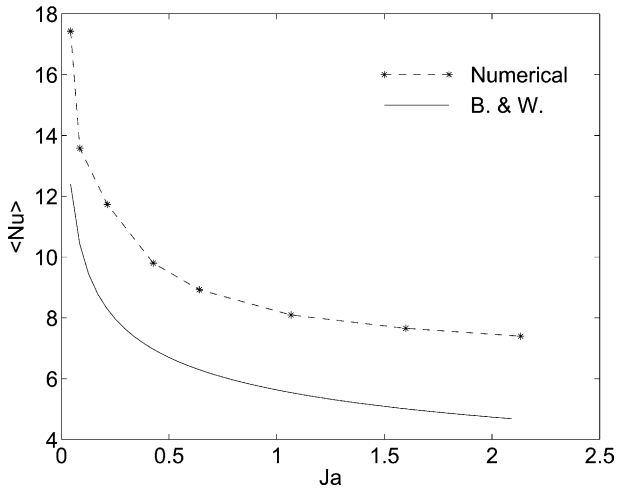

Fig. 5. Variation of $\overline{\langle Nu \rangle}$ with Ja. Here, $Gr = 1680$, $\widetilde{D} = 1.55$, and other thermophysical properties are $\rho_l/\rho_v = 4.78$, $\mu_l/\mu_v = 2.59$, $k_l/k_v = 3.553$, $c_l/c_v = 0.546$ and $Pr = 4.2$.

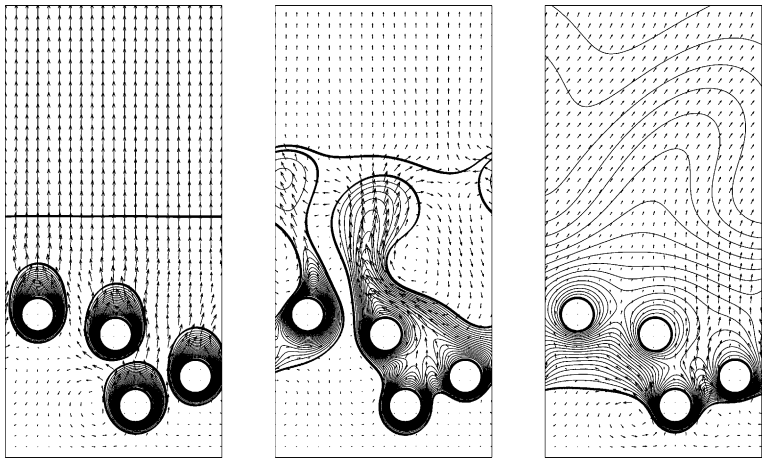

Fig. 6. Evolution of a highly unsteady liquid/vapor phase boundary during film boiling on multiple horizontal cylinders. Here, the thermophysical parameters are the same as in Fig. 5 except $Gr = 67.2$ and $Ja = 1.06$. The figure shows the phase boundary along with the temperature contours and the velocity vectors (at every sixth grid point). The frames proceed from the left to the right.

the temperature contours and a vector plot of the velocity field (plotted at every sixth grid point) at three selected times. Initially each phase boundary grows similarly to that of an isolated cylinder. However, as the phase boundaries expand more, they start to interact and eventually coalesce. This results in the formation of the large vapor region seen in frame (2) which completely encompasses the cylinders. As the vapor plumes grew larger, they coalesce with the top interface. At this point, most of the domain is occupied with vapor except for a small region near the lower wall and two isolated islands of liquid in the middle of the domain (not shown here). The liquid

islands finally disappear with further evaporation (frame 3). The figure shows a gradual decrease in the magnitude of the velocity field as the process continues. This is due to the fact that the temperature gradient in the vapor, which drives the flow, starts to diminish as the vapor layer gets thicker. This can be seen clearly by inspection of the temperature field. Overall, this simulation shows the feasibility of studying complex problems where frequent topology changes necessitate the use of a robust and easy to implement numerical technique.

4. Conclusion

We have developed a front tracking method for computations of boiling in complex geometries. The method is well-suited for incorporating arbitrary solid boundaries into the flow field in Cartesian grid computations. We conducted two validation tests and a grid resolution study to test the performance of the energy equation and the momentum solver against available exact solutions and to show the convergence of the method under grid refinement. We also presented film boiling simulations on a horizontal cylinder and multiple cylinders which test the full phase change algorithm. While these tests show that the method is robust and converges as the grid is refined, they also show that it demands a relatively high grid resolution. This calls for implementation of an adaptive mesh refinement, similar to the one used by Agresar et al. (1998), where the grid points are clustered near the solid. Despite this shortcoming, we believe that these computations show the feasibility of simulating film boiling in complex geometries.

Acknowledgements

This work was supported by NASA Microgravity program under grant numbers NAG3-2583 and NAG3-2545.

References

Adams, J., 1989. MUDPACK: multigrid FORTRAN software for the efficient solution of linear elliptic partial differential equations. Appl. Math. Comput. 34, 113–146.

Agresar, G., Linderman, J.J., Tryggvason, G., Powell, K.G., 1998. An adaptive, Cartesian, front tracking method for the motion, deformation and adhesion of circulating cells. J. Comput. Phys. 43, 346.

Al-Rawahi, N., Tryggvason, G., 2002. Numerical simulation of dendritic solidification with convection: Two-dimensional geometry. J. Comput. Phys. 180, 471–496.

Beckermann, C., Diepers, H.-J., Steinbach, I., Karma, A., Tong, X., 1999. Modeling melt convection in phase-field simulations of solidification. J. Comput. Phys. 154, 468–496.

Breen, B.P., Westwater, J.W., 1962. Effect of diameter of horizontal tubes on film boiling heat transfer. Chem. Eng. Progr. 58, 67–72.

Bromley, L.A., 1950. Heat transfer in stable film boiling. Chem. Eng. Progr. 46, 221–227.

Capone, G.J., Park Jr., E.L., 1970. Estimation of film-boiling heat transfer coefficients for cylindrical heater in corresponding-state fluids. Adv. Cryog. Eng. 15, 283–285.

Carey, V.P., 1992. Liquid–vapor phase-change phenomena. Taylor and Francis, London.

Drummond, J.E., Tahir, M.I., 1984. Laminar viscous flow through regular arrays of parallel solid cylinders. Int. J. Multiphase Flow 10, 515–540.

Esmaeeli, A., Tryggvason, G., 2003. Computations of explosive boiling in microgravity. J. Scient. Comput. 19, 163–182.
Esmaeeli, A., Tryggvason, G., 2004a. Computations of film boiling. Part I—Numerical method, Int. J. Heat Mass Transfer (to appear).
Esmaeeli, A., Tryggvason, G., 2004b. Computations of film boiling. Part II—Multimode film boiling, Int. J. Heat Mass Transfer (to appear).
Fadlun, E.A., Verzicco, R., Orlandi, P., Mohd-Yusof, J., 2000. Combined immersed-boundary finite-difference methods for three-dimensional complex flow simulations. J. Comput. Phys. 161, 35–60.
Goldstein, D., Handler, R., Sirovich, L., 1993. Modeling a no-slip flow boundary with an external force field. J. Comput. Phys. 105, 354.
Incropera, F.P., DeWitt, D.P., 2002. Fundamentals of heat and mass transfer, Fifth ed. John Wiley and Sons, New York.
Juric, J., Tryggvason, G., 1998. Computations of boiling flows. Int. J. Multiphase Flow 24, 387–410.
Kirkpatrick, M.P., Armfield, S.W., Kent, J.H., 2003. A representation of curved boundaries for the solution of the Navier–Stokes equations on a staggered three-dimensional Cartesian grid. J. Comput. Phys. 184, 1–36.
Lienhard, J.H., Sun, K.-H., 1970. Effect of gravity and size upon film boiling from horizontal cylinders. J. Heat Trans. 92, 292–298.
Leonard, B.P., 1979. A stable and accurate convective modeling procedure based on quadratic upstream interpolation. Comput. Methods Appl. Mech. Eng. 19, 59–98.
Ozisik, M.N., 1980. Heat conduction. Wiley Interscience Publication, New York.
Sangani, A.S., Acrivos, A., 1982. Slow flow past periodic arrays of cylinders with application to heat transfer. Int. J. Multiphase Flow 8, 193–206.
Shin, S., Juric, D., 2002. Modeling three-dimensional multiphase flow using a level contour reconstruction method for front tracking without connectivity. J. Comput. Phys. 180, 427–470.
Son, G., Dhir, V.K., 1998. Numerical simulation of film boiling near critical pressures with a level set method. J. Heat Trans. 120, 183–192.
Tryggvason, G., Bunner, B., Esmaeeli, A., Juric, D., Al-Rawahi, N., Tauber, W., Hans, J., Nas, S., Jan, Y.-J., 2001. A front-tracking method for the computing of multiphase flow. J. Comput. Phys. 169, 708–759.
Welch, S.W.J., Wilson, J.J., 2000. A volume of fluid based method for fluid flows with phase change. J. Comput. Phys. 160, 662–682.